Theses and Dissertations

May 2013

DC Microgrid Modeling and Energy Storage Placement to Enhance System Stability

Carl Westerby
University of Wisconsin-Milwaukee

www.manaraa.com

DC MICROGRID MODELING AND ENERGY STORAGE PLACEMENT TO ENHANCE SYSTEM STABILITY

by

Carl Westerby

A Thesis Submitted in
Partial Fulfillment of the
Requirements for the Degree of

Master of Science
in Engineering

at

The University of Wisconsin-Milwaukee

May 2013

ABSTRACT

DC MICROGRID MODELING AND ENERGY STORAGE PLACEMENT TO ENHANCE SYSTEM STABILITY

by

Carl Benjamin Westerby

The University of Wisconsin-Milwaukee, 2013
Under the Supervision of David Yu, PhD

The work of this thesis represents a joint venture between the University of Wisconsin-Milwaukee and the University of Wisconsin-Madison. A DC microgrid is selected for the efficiency benefits, lack of reactive power in the system, and ease of connecting to an AC grid. The system modeling relies on physical parameters and industry standard methods for the estimation of loads and lines. An example model is created for the University of Wisconsin - Milwaukee's Campus. Due to the high penetration of renewable energy sources in the example model, system stability is a concern. To help mitigate stability issues, analysis is performed to have the ideal placement of energy storage. The analysis relies heavily on the deep properties of the system such as Eigenvalues and system controllability. Energy storage placement is verified and evaluated with model simulations.

www.manaraa.com

Dedicated to Talia, Jane, and Bryan.

"Courage is not simply one of the virtues, but the form of every virtue at the testing point."

-C. S. Lewis

With enough voltage everything conducts electricity.

TABLE OF CONTENTS

LIST OF FIGURES

LIST OF TABLES

ACKNOWLEDGMENTS

I want to dedicate this work to my family, whose support was instrumental in the completion of this work. Without them, I would not be the man that I am today. I also thank God for the opportunities that he has given me. I owe a special thanks to Professor David Yu who has been my advisor throughout the process. His financial support and guidance during my graduate studies have been instrumental in the completion of this work. I would also like to thank Dr. Nasiri and Dr. Hosseini for serving on my Master's Degree thesis defense committee.

I appreciate the assistance provided by our colleagues at the University of Wisconsin – Madison. Professor Yehui Han and his group were very helpful in the selection of converter topology used and in modeling the converters. Thank you to all of the members of my own research group here in Milwaukee. A special thanks to Qiang Fu, who has provide loads of guidance and been a great sounding board for my ideas.

1 Introduction

With a recent push for clean and renewable sources of energy, the popularity of microgrids has increased significantly. [1] Microgrids can provide a great option for integrating localized renewable generation. Power quality and reliability can be insured with energy storage and generators to support loads through the loss of a renewable source. While the majority of microgrid research is focused on alternating current (AC) systems, direct current (DC) offers many advantages.

For instance, the system efficiency is boosted by reducing the losses created by conversion from DC to AC. Since the voltage is constant, the system does not have reactive power and is therefore simpler. Also, when connecting to an AC utility there is no need to worry about synchronization, since the microgrid does not have a frequency. While there are many advantages of DC microgrids, stability is concern due to the high penetration and variability of renewable resources. The loss of power for even small periods can be an incredible nuisance for the consumer. Frequent power outages disrupt customer activity but can be particularly troublesome on a college campus, as outages may destroy research efforts. In order to prevent stability issues, energy storage is incorporated into the microgrid. Energy storage, such as batteries, work by injecting current into the system during periods when renewable resources are unavailable. Energy storage is not free, so optimal placement of storage can reduce system installation costs.

This thesis documents techniques for creating a dynamic system model. The process relies heavily on physical information such as estimated cable distances and building footprints. A Dual-Active Bridge (DAB) DC-DC converter technology is used to connect sources and loads to the grid. This converter topology is included in the system modeling. The final focus of this paper is analyzing the system to achieve optimal placement of energy storage. The methodology relies on the properties of the state space model for the system. The system's controllability is considered in order to maintain the voltage. Additionally, system eigenvalues are used to help determine the placement of energy storage. The results of the analysis are evaluated using simulations of the system model.

2 System Interconnection and Load Parameters

The system modeling is based on distances from satellite images. The distances between buildings can be used to estimate resistance and inductance values.
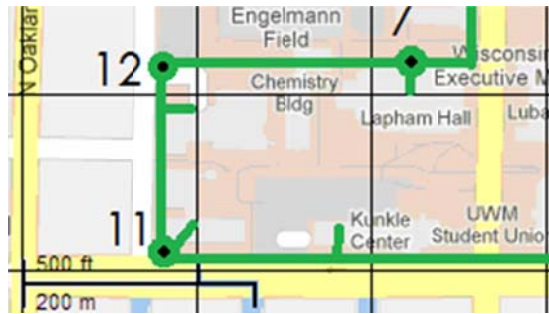
Figure 2.1 Cable Distance

Shown below is the equation for resistance based on conductor area (A), length of the cable (l), and resistance density of copper (ρ).

$$(2.1) \qquad R_{dc} = \frac{\rho l}{A}$$

If multiple cables are used, the composite resistance is calculated using the formula for equivalent parallel resistors.

$$(2.2) \qquad R_{composite} = \frac{R_{cable}}{N_{cables}}$$

The inductance for the cables can be calculated using the geometric mean distance (GMD), the geometric mean radius (GMR), and distance (d) in meters.

$$(2.3) \qquad L = \left(\frac{\mu_o}{2\pi}\right) \ln\left(\frac{GMD}{GMR}\right) d$$

The GMD for a single conductor, in a multi-conductor cable, can be approximated as shown in equation (2.4) where D_{1N} represents the distance from conductor 1 to the Nth conductor at the same voltage level. The GMS is the geometric mean distance of a single conductor.

$$(2.4) \qquad GMD_1 = \{(GMS)(D_{12})(D_{13}) \dots (D_{1N})\}^{1/N}$$

The GMS of a single circular conductor is calculated using (2.5), where r is the radius of a conductor.

$$(2.5) \qquad GMS = re^{-0.25} \text{ [2]}$$

The GMD for the multi-conductor cables is the geometric mean of the GMD of all conductors, as shown in (2.6).

$$(2.6) \qquad GMD_{cable} = \{(GMD_1)(GMD_2)(GMD_3) \dots (GMD_N)\}^{1/N} \text{ [2]}$$

The GMR for a multiconductor cable is similar to the GMD. Except that it is the distance to cables at different potentials. Equation (2.7) illustrates this relationship, where D_{1N} represents the distance from the first cable to the N_{th} cable at a different voltage potential.

$$(2.7) \qquad GMR_1 = \{(D_{11})(D_{12}) \dots (D_{1N})\}^{1/N} \text{ [2]}$$

The composite GMR is the geometric mean of the individual conductors' GMR.

$$(2.8) \qquad GMR_{cable} = \{(GMR_1)(GMR_2) \dots (GMR_N)\}^{1/N}$$

The interconnection cables are sized using the National Electrical Code (NEC). Table 2.1 gives ampacity limitations for different sizes of conductors. By

knowing the maximum current that can flow between different nodes, the number

and size of each conductor in the cable can be determined.

Conductor Size	Copper Ampacity (A)	Aluminum Ampacity (A)
2000 MCM	665	560
1500 MCM	625	520
1250 MCM	590	485
1000 MCM	545	445
750 MCM	475	385
500 MCM	380	310
250 MCM	255	205

Table 2.1 Cable Ampacities

The loads for each building can be estimated based on square footage.

The National Electrical Code (NEC) states that in new building design, lighting

load should be estimated at 3 VA/ft^2 and the receptacle loads can be estimated

at 1 VA/ft^2 for office buildings.[3] Many contractors use an HVAC sizing rule of

thumb of 600 ft^2/ton[4], equivalent to 0.9 watt/ft^2. Building square footage can be

estimated from the building foot print satellite images.
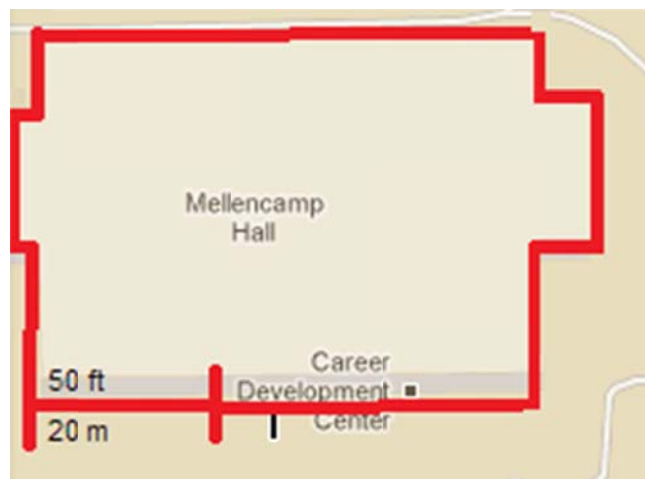
Figure 2.2 Building Square Footage

The number of floors can be counted by using satellite images to zoom in on each building.
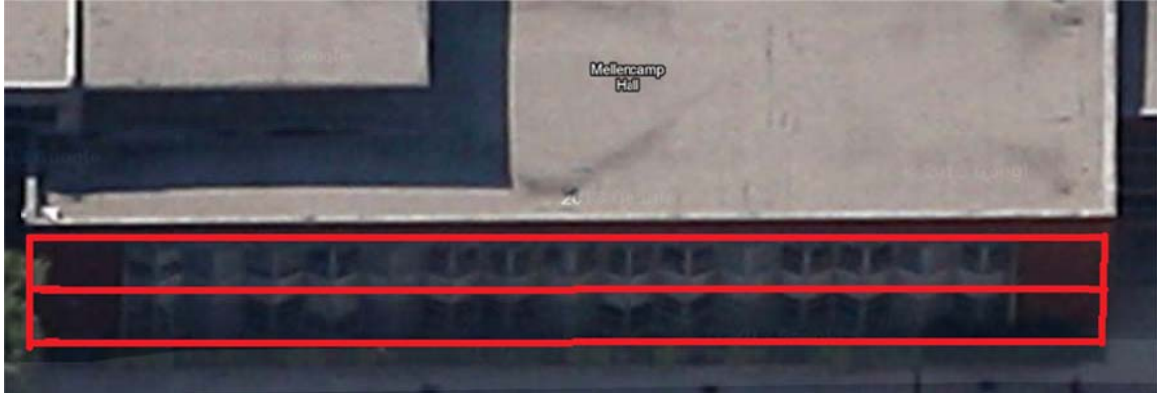
Figure 2.3 Number of Stories

Using the number of stories (N_s) and footprint (A) gives a total building square footage. This number multiplied by the square footage loading values for lighting, office receptacles, and HVAC provides an estimate for loading.

$$(2.9) \qquad P_{load} = A(N_s)(3.0 + 1.0 + 0.9)$$

A rule of thumb of 8 watt/ft^2 is used to estimate the amount of solar power each building can provide with solar panels more or less covering the roof. This value is taken at 80% of an NREL study done in Middleton Wisconsin.[5] The value of 8 watt/ft^2 plus the footprints previously calculated will be used to represent the typical solar panel each building can provide.

3 Dual Active Bridge Converter Topology

DC-DC switch mode converters will be used in the system to convert from different voltage levels. The converter topology selected is a DAB. The DAB was selected because it is a mature topology, it provides electrical isolation between the input and the output, and it has good power efficiency. The converter has a 4 switch active H-bridge at the input and output. The dual H-bridges are the source of its name. The output is isolated with a high frequency transformer.
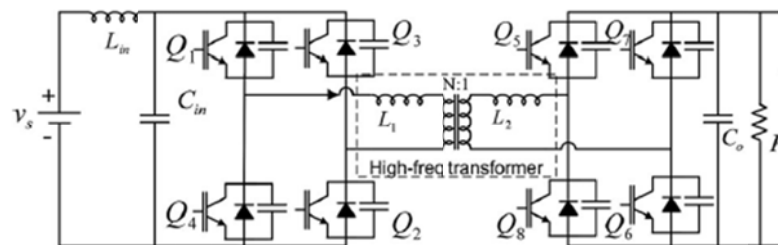
Figure 3.1 DAB Schematic[6]

The converter boosts the voltage between the input and the output via the turns ratio of the high frequency transformer. Both bridges are operated at a 50% duty cycle and generate a square wave that oscillates between $+V_{dc}$ and $-V_{dc}$.

Power flow is controlled by the phase delay between the input and output bridges. The high frequency transformer is designed with a specific series inductance (L_S). An additional series inductor may also be added to achieve the desired value. As shown in equation (3.1) the change in the inductor current is proportional to the voltage drop across the inductor.

$$(3.1) \qquad V_L = L_s \frac{\Delta i_L}{\Delta t}$$

As seen in Figure 3.2, during the time I, when the primary voltage lags the secondary voltage there is a rise in inductor current. During this time the voltage drop across the series inductance is the input voltage plus the output voltage.

$$(3.2) \qquad V_{L1} = V_{in} - (-V_{out})$$

During time II, when the secondary voltage is positive, the voltage drop is the input voltage minus the output voltage.

$$(3.3) \qquad V_{L2} = V_{in} - V_{out}$$

This causes a smaller rise in inductor current.
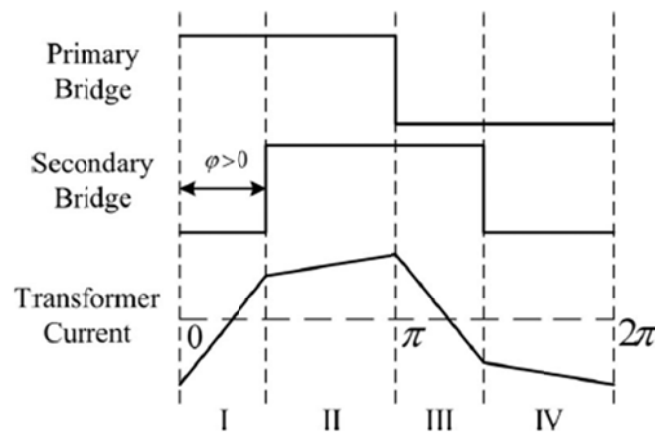
Figure 3.2 DAB Voltage Waveforms[6]

Segments III and IV are the same as I and II, but the output voltage and current are in the opposite direction, in order to balance out the average current through the inductor. By increasing the phase lag between the primary and secondary voltages, the inductor current will have a longer time to rise. This results in a larger rise and an increase in power transfer from primary to secondary.

The output power for the converter is shown in equation (3.4).

$$(3.4) \qquad P = \frac{V_{in}V_{out}}{2Nf_{sw}L_s}d(1-d) \quad [6]$$

This equation depends on the input and output voltages (V_{in} and V_{out}), turns ratio (N), switching frequency (f_{sw}), series inductance (L_s), the phase shift (d) between primary and secondary voltages. In equation (3.4) the phase shift is represented as the phase angle in radians divided by π.

Since any large system will have many DAB converters, a reduced order model is needed. A simplified model is presented in [7] which uses a current source, output capacitor, and resistive load. The schematic is shown in Figure 3.3.
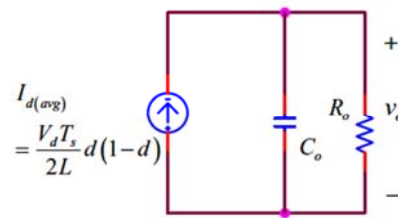
Figure 3.3 Reduced Order DAB Model[7]

This model can be combined with system parameters of the previous chapter in order to give a complete system. The details of this approach are provided in the following chapter.

4 Dynamic System Modeling

The system model combines the methods discussed previously. Nodes or busses represent a connection point for multiple building loads and distributed generation sources. Loads are modeled as resistors, and sources are modeled as capacitors with current sources. Multiple loads at a single node are combined as resistors in parallel to give a composite resistance. The same is down for multiple sources connected at a node. The capacitance values are added in parallel and the current source size is increased accordingly. Nodes are connected by a resistor and inductor, which represent the cable impedances. Figure 4.1 shows an example of a system with 3 busses and two interconnections.
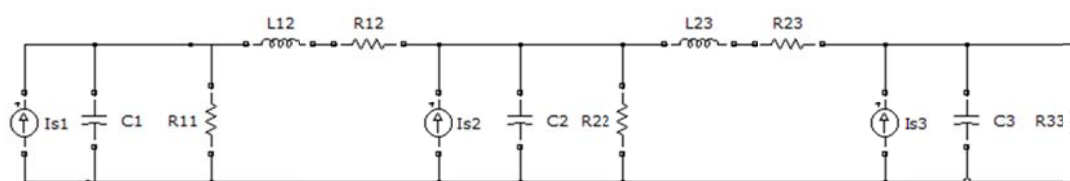
Figure 4.1 Simple 3 Bus System Example

A dynamic model of the system can be created by examining the differential equations. Using Kirchhoff's Current Law (KCL) at each node, the capacitor voltage can be described by a differential equation. Figure 4.2 shows an example equation for the first node in the simple 3 bus system.
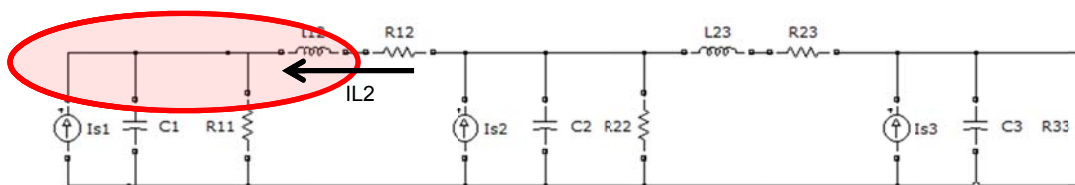
$$\frac{dV_1}{dt} = \frac{-V_1}{C_1 R_{11}} + 0V_2 + 0V_3 + \frac{I_{L12}}{C_1} + 0I_{L23} + \frac{I_{s1}}{C_1}$$

Figure 4.2 Example KCL Differential Equation

The resistor current is the node voltage divided by the resistance. The Node voltages from the other two nodes do not contribute. Current flowing through the

interconnecting line and from the current source also flow into the capacitor. The capacitor current is then replaced by the capacitance times the derivative of the voltage. Finally, the capacitance is divided on both sides of the equation.

The current in the inductor provides another differential equation using Kirchhoff's Voltage Law (KVL) around a loop containing the inductor voltage. An example is shown in Figure 4.3.

$$\frac{dI_{L12}}{dt} = \frac{V_1}{L_{12}} - \frac{V_2}{L_{12}} + 0V_3 - \frac{I_{L12}R_{12}}{L_{12}} + 0I_{L23}$$
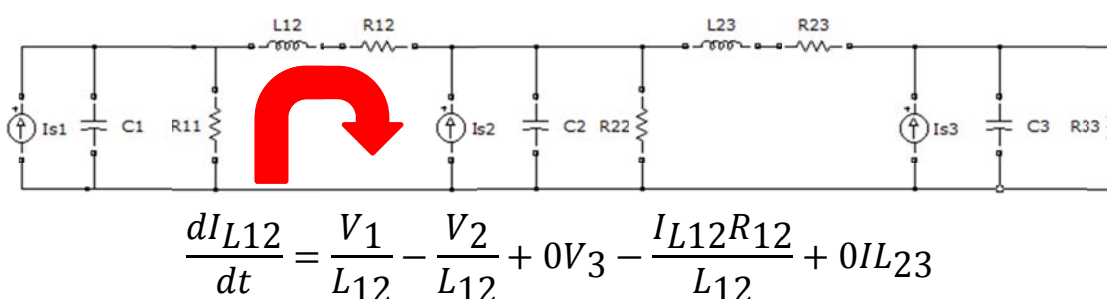
Figure 4.3 KVL Example

The inductor voltage drop is equivalent to V1 minus V2 minus the voltage drop in the resistor. The inductor voltage is replaced by the inductance times the derivative of the current, and both sides of the equation are divided by the inductance.

After deriving all the equations for the capacitor voltages and inductor currents, the differential equations can be combined into a state space model. Each node voltage and line current is chosen to be a state variable, and the current source at each node is considered an input to the system. The dynamic system typical state space model is shown (4.1), where x represents the column matrix of the system states and u is the column matrix of the system inputs.

$$(4.1) \qquad \dot{x} = A_p x + B_p u$$

In the instance of the three bus system, the complete state-space model is shown in Figure 4.4.

$$
\begin{bmatrix} \dot{V}_1 \\ \dot{V}_2 \\ \dot{V}_3 \\ \dot{I}_{L12} \\ \dot{I}_{L23} \end{bmatrix} = \begin{bmatrix} -1/C_1 R_{11} & 0 & 0 & 1/C_1 & 0 \\ 0 & -1/C_2 R_{22} & 0 & -1/C_2 & 1/C_2 \\ 0 & 0 & -1/C_3 R_{33} & 0 & -1/C_3 \\ -1/L_{12} & 1/L_{12} & 0 & -R_{12}/L_{12} & 0 \\ 0 & -1/L_{23} & 1/L_{23} & 0 & -R_{23}/L_{23} \end{bmatrix} \begin{bmatrix} V_1 \\ V_2 \\ V_3 \\ I_{L12} \\ I_{L23} \end{bmatrix}
$$

$$
+ \begin{bmatrix} 1/C_1 & 0 & 0 \\ 0 & 1/C_2 & 0 \\ 0 & 0 & 1/C_3 \\ 0 & 0 & 0 \\ 0 & 0 & 0 \end{bmatrix} \begin{bmatrix} I_{s1} \\ I_{s2} \\ I_{s3} \end{bmatrix}
$$

Figure 4.4 State Space Model for a 3 Bus System

5 UWM System Model

Using the techniques and methodologies from the previous chapters, a 12 bus system model is created for the University of Wisconsin - Milwaukee campus. Figure 5.1 shows the physical layout of the system.

Figure 5.1 UWM System Map

Each number represents a bus. Bus 1 represents the collection point for multiple offshore wind turbines located in Lake Michigan. It supplies around 3 MW.

Once the physical layout has been determined, one of the most important properties of the system will be the voltage level. The selection of a system voltage is difficult due to many competing factors such as efficiency, safety, and various standards. Figure 5.2 overviews various voltage levels, standards, implementations, and benefits. The main voltage constraint in the US is the NEC's 600 V maximum for low voltage in residential areas. Equipment also becomes more expensive when the voltage rating goes above 600V.
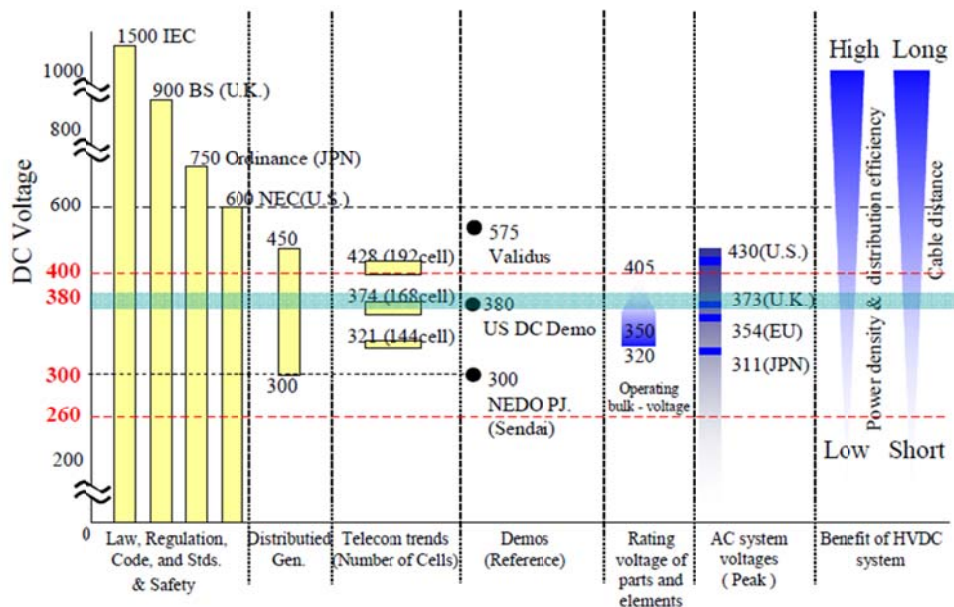
Figure 5.2 Voltage Overview[8]

The figure has 380 volts highlighted because it is below the 600 volt maximum, but still provides good efficiency. Additionally, there is an ETSI Standard in progress for the 380 VDC voltage level (EN 300 132-3-1)[8] . Several telecommunication facilities adopted this voltage level as well.
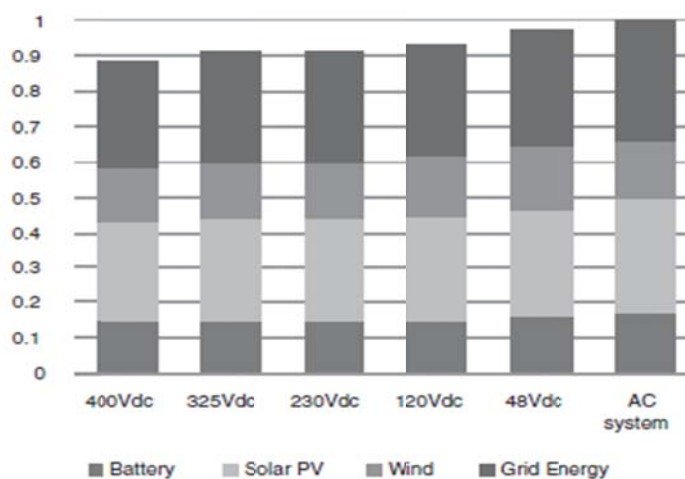
Figure 5.3 Comparison of Energy Usage for Different System Voltages[9]

Figure 5.3 shows the estimated energy usage for various voltages. The 400 VDC

system uses less than 90% of the energy in a traditional AC system.[9] For all of

these benefits, the system voltage level will be 380 V.

In order to complete the model, system parameters need to be calculated

from the physical dimensions. The areas for the buildings are estimated from

satellite images; the solar capacity and load estimate are created using the

square footage and techniques described in previous sections.

Name	Area (ft^2)	Stories	Total Area (ft^2)	Load (kW)	Solar(kW)	Bus #
Physics Building 1	12500	4	50000	245	90	11
Physics Building 2	7500	1	7500	36.75	54	11
EMS	5000	11	55000	269.5	36	12
EMS small	7500	3	22500	110.25	54	12
Kunkle Center	28125	3	84375	413.4375	202.5	11
UWM Union	75000	3	225000	1102.5	540	10
Vogel and Curitn	10000	9	90000	441	72	9
Mitchell Hall	22500	3	67500	330.75	162	9
Mellencamp Hall	10000	2	20000	98	72	9
Art Building	30000	3	90000	441	216	9
Pearse and Garland Hall	15000	4	60000	294	108	8
Johnston and Holton Hall	10000	3	30000	147	72	2
Sabin Hall	10000	4	40000	196	72	6
Klotsche	20000	2	40000	196	144	6
Pavillion	30000	2	60000	294	216	6
Library	80000	2	160000	784	576	3
Ender Hall	10000	11	110000	539	72	3
Norris Health Center	2500	2	5000	24.5	18	3
Chapman Hall	625	4	2500	12.25	4.5	4
Architechure Building	7500	4	30000	147	54	5
Engleman and Cuningham Hall	28125	3	84375	413.4375	202.5	5
Lapham Hall	7500	5	37500	183.75	54	7
Lubar Hall	25000	5	125000	612.5	180	7
Chemistry Building	11250	4	45000	220.5	81	12

Table 5.1 Summary of Loading and Solar Capacity per Building

Table 5.2 shows the solar capacity and load per bus. The resistance is calculated using load in kW and the bus voltage of 380 V.

Bus	Bus Load (kW)	R_{load} (ohms)	Generation (kW)	# of Converters	C (F)
1	Line Parasitics	1000	3000	15	0.015
2	147	0.982	147	7	0.007
3	1347.5	0.107	650	33	0.033
4	12.25	11.788	0	1	0.001
5	560.44	0.258	250	13	0.013
6	686	0.210	420	21	0.021
7	796.25	0.181	230	12	0.012
8	294	0.491	100	5	0.005
9	1310.75	0.110	510	26	0.026
10	1102.5	0.131	540	27	0.027
11	695.2	0.208	34	2	0.002
12	600.25	0.241	160	8	0.008

Table 5.2 Bus Summary of Loading and Solar Capacity

The capacitance is calculated using the number of converters and an individual converter capacitance of 1 mF.

The distances between busses are measured and used to calculate cable distances. The cables are sized for 3 MW since the cables are radially fed, with a near equal split at Bus 2. In order to meet the ampacity requirements a quantity of 12, 2000 kcmil cables are used. The cables are spaced in a duct bank using the NEC rules for percent conduit fill and conduit spacing.[3] The layout is shown in Figure 5.4.
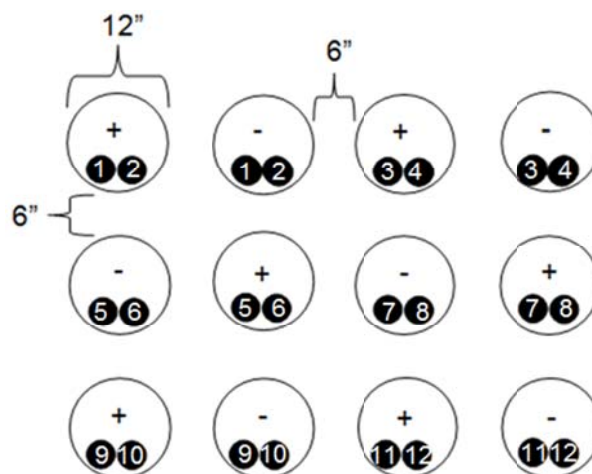
Figure 5.4 Conduit Layout

The inductance can be calculated for each cable using equations (2.3) through

(2.8). The conductors are numbered from left to right and top down with numbers

repeating for each polarity. The GMS of an individual conductor is 1.27 inches,

using equation (2.5) the radius of 1.632 inches. Table 5.3 shows an example

GMD calculation for the first two conductors, which are approximately equal.

	D1	D2	D3, D4, D9, D10	D5, D6	D11, D12	D7, D8	GMD
Cond1≈ Cond2	ds	2	6*6	18√2	2*18√2	√(4.5^2+1.5^2)*12	**23.11**
	1.27	2	36	25.46	50.91	56.88	

Table 5.3 Sample GMD calculation for Conductors 1 and 2

Table 5.4 shows a sample calculation for the GMR of conductors 1 and 2. The

difference between the GMD and GMR is the GMD uses distances between all

the positive voltage cables, and the GMR uses the distance from each positive

cable to all the other phase cables (negative voltage).

	D1, D2, D5, D6	D3, D4	D7, D8, D9, D10	D11, D12	GMR
Cond1≈	6*3	6*9	5.25*12	5.41*12	**40.64**
Cond2	18	54	63	64.92	

Table 5.4 Sample GMR Calculation for Conductors 1 and 2

Table 5.5 tabulates the individual conductor GMR and GMD. It also shows the composite values for the entire cable. The cable composite is calculated as the geometric mean of the individual conductors.

	1 & 2	3 & 4	5 & 6	7 & 8	9 & 10	11 & 12	Cable Composite
GMD	23.11	20.21	16.99	22.22	23.11	20.21	**20.86**
GMR	40.64	33.67	27.33	32.82	40.64	33.67	**34.48**

Table 5.5 Composite Cable GMD and GMR

The inductance per foot is calculated using equation (2.3). Table 5.6 details the calculation. Using the result of Table 5.6 and the line distances measured from the map, the interconnection cable distances can be calculated.

GMD	GMR	μo/2π	ft/m	L/d=(μo/2π)ln(GMD/GMR)/(ft/m)
20.86	34.48	2.00E-07	3.28	-3.06E-08 H/ft

Table 5.6 Inductance per Foot

The resistance per foot is calculated using the individual conductor resistance and number of conductors. In this case the resistance per foot is calculated using an ohmic density of copper equal to 10.371 and 2 million circular mils of the 2,000 MCM cable. With 12 conductors, the value is 0.864 micro-ohms per foot. Table 5.7 summarizes the cable inductance and resistances for the 12 bus system.

Name	Distance (feet)	R (Ω)	L (H)
Bus 1-2	3000	0.0051855	9.38E-05
Bus 2-3	500	0.00086425	1.56E-05
Bus 2-6	500	0.00086425	1.56E-05
Bus 3-4	625	0.001080313	1.95E-05
Bus 4-5	300	0.00051855	9.38E-06
Bus 5-7	600	0.0010371	1.88E-05
Bus 2-8	300	0.00051855	9.38E-06
Bus 9-8	600	0.0010371	1.88E-05
Bus 10-9	1100	0.00190135	3.44E-05
Bus 11-10	1600	0.0027656	5.00E-05
Bus 12-11	600	0.0010371	1.88E-05

Table 5.7 System Impedances

Using the system parameters of line inductance, line resistance, node
resistance (load), and node capacitance, a state space model of the system is
created using equation (4.1). A 23 x 23 A_p matrix is created with a differential
equation for each node voltage (x12) and each line current (x11). The voltage
differential equation can be defined solely using the states, with the exception of
the current injection at each bus. The current injection is chosen to be the system
input and results in a B_p matrix which is highly sparse. It only has values along
the diagonal that are equal to 1 divided by the capacitance at that bus. The
Model is similar to Figure 4.4 but much larger.

6 System Analysis

System stability is important, because the owner of the microgrid does not make any money if the microgrid is down. Prolonged outages also create angry customers. With a high penetration of renewable energy, system voltages and currenets can drop quickly unless corrective action is taken. One form of corrective action is adding energy storge. During times when renewables generate excess power the batteries store the energy, and when the wind stops or sun is blocked, the batteries output power to the microgrid. Energy storage is not cheap, and in order to achieve the maximum system impact for the lowest cost, care must be taken to place energy storage in the correct location.

In order to analyze the system, the differential equations that comprise the state space model are borken into two parts as in equation (6.1).

$$(6.1) \qquad \dot{x}(t) = A_p[x(t)] + B_p[u(t)]$$

The first part of the equation is the system Matrix (A_p) and it relates the current values of the states to the differential change in the states. This type of analysis deals with system dynamics in order to see which nodes are the most unstable. The second part of the analysis is related to how the input (u) affects changes to the states (B_p). This type of analysis will show which node gives the best bang for the buck in terms of current injection to change in node voltages.

A major method of analyzing the system matrix (A_p) is to look at the eigenvalues. The system eigenvalues derive from the fact the system is

composed of differential equations. Linear differential equations have solutions that take the form shown in equation (6.2).

$$(6.2) \qquad x = x_o e^{\lambda t}$$

In order for the solution to have bounded input bounded output (BIBO) stability, the eigenvalue (λ) must be negative to make the expontial decaying . The 12 bus system's eigenvalues are plotted in Figure 6.1. The real values are on the x-axis and the imaginary values are plotted on the y-axis. Since the system has all negative real values, it is BIBO stable.

Figure 6.1 Twelve Bus System Eigenvalue Plot

The damping and speed of the system modes will be key in determing dynamic system response and stability. The damping ratio is a dimensionless measure of describing the decay of oscilations in the system modes. Values less than 1 corespond to underdamped systems, which will have overshoot and oscilations. A damping of greater than 1 describes an overdamped system which

will not oscilate or overshoot, but will exponentially decay or increase to its equilibrium position. The equation for calculating system damping is shown in equation (6.3), where the eigenvalue is defined as a ± bj.

$$(6.3) \qquad \zeta = \frac{a}{\sqrt{a^2+b^2}}$$

Lightly damped system eigenvalues will be the modes of the system that are most likely to make the system unstable. The system damping values for the 12 bus system are shown in Figure 6.2. Both bus voltages and line currents are shown, since they comprise the states of the system.
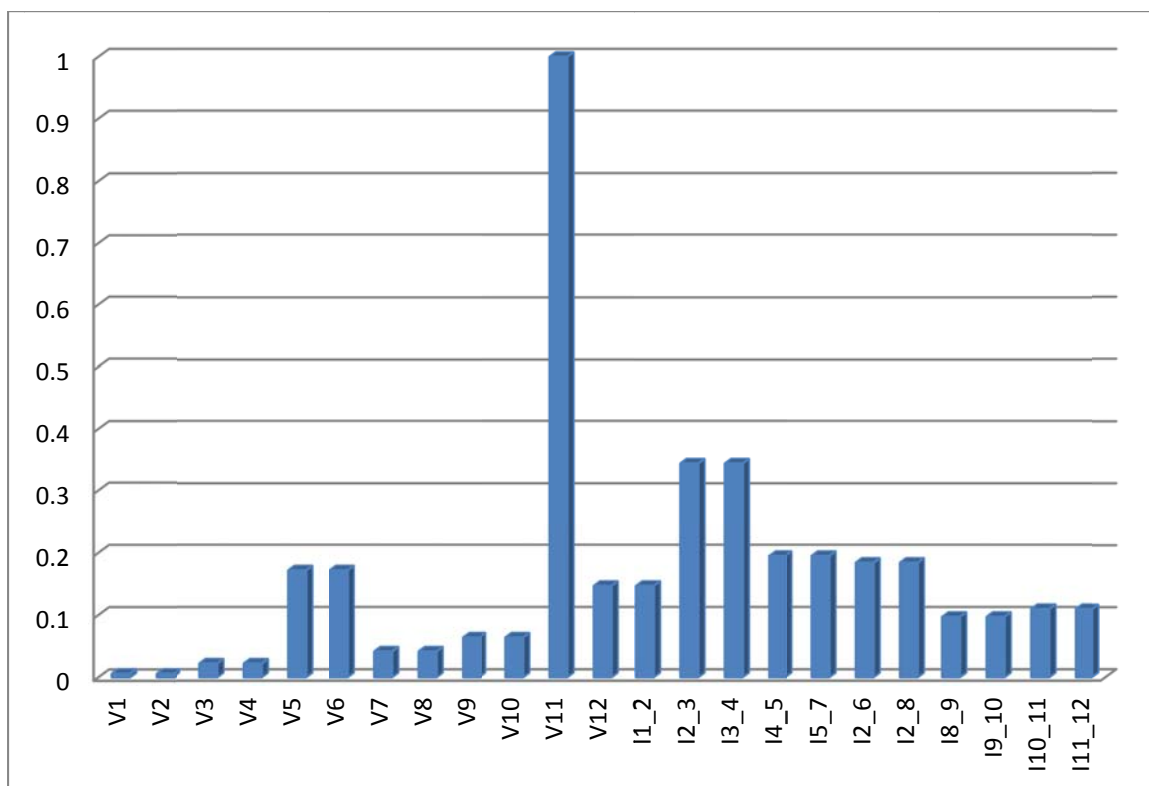
Figure 6.2 System Damping

Since all the eigenvalues, except the voltage at bus 11, have imaginary parts they are underdamped. The voltage in busses 1-4 and 7-8 have the lightest

damping (under 0.05), and are the best candinates for battery placement. Another parameter to consider is system speed.

The eigenvalues each have a natural frequency. The natural frequency can be calculated using equation (6.4).

$$(6.4) \qquad \omega_n = \sqrt{a^2 + b^2}$$

The speed of the system eigenvlaues is shown in Figure 6.3.
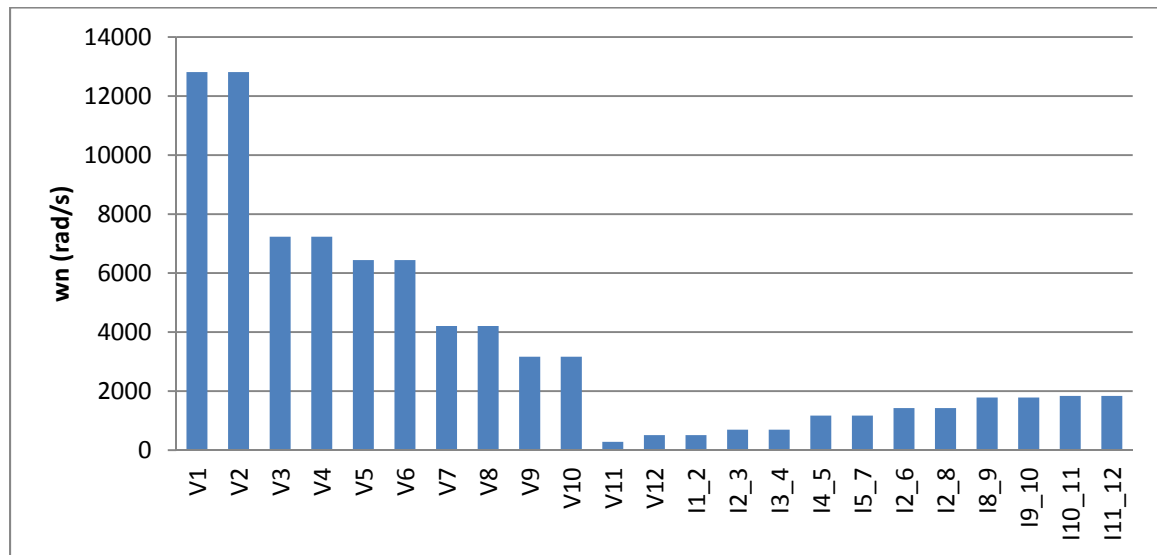
Figure 6.3 System Eigenvalue Natural Frequency

The voltages with the lowest speed will be more dominant modes, because it will take longer for their oscilations to cease. Of the busses that are the most lightly damped, Bus 7 and Bus 8 are the slowest making them likely candiates for the most unsatble bus.

In order to consider how the input affects the change of states, the system must be converted to modal coordinates. Equations (6.5), (6.6), and (6.7) give the formulas for the change of basis, using the eigenvectors (V) as the basis vectors.

$$(6.5) \qquad A_m = V^{-1}A_pV$$

$$(6.6) \qquad B_m = V^{-1}B_p$$

$$(6.7) \qquad C_m = C_pV$$

In modal coordinates the systems modes are decoupled, so they can be considered independently. If any of the modes are unaffected by the control input, then the system is uncontrollable. If the system is uncontrollable, changes in the system conditions may cause the system to become unstable with no way of performing corrective action.

The magnitude of the B_m matrix for the 12 bus system is shown in Table 6.1.

	Bus 1	Bus 2	Bus 3	Bus 4	Bus 5	Bus 6	Bus 7	Bus 8	Bus 9	Bus 10	Bus 11	Bus 12
Eig 1	0.00	3.25	45.14	4664.25	252.04	0.00	7.01	0.50	0.00	0.00	0.00	0.00
Eig 2	0.00	3.25	45.14	4664.25	252.04	0.00	7.01	0.50	0.00	0.00	0.00	0.00
Eig 3	18.36	1329.51	52.26	21.00	4.33	82.36	0.40	1422.01	59.23	1.25	0.62	0.08
Eig 4	18.36	1329.51	52.26	21.00	4.33	82.36	0.40	1422.01	59.23	1.25	0.62	0.08
Eig 5	0.00	0.45	0.01	0.00	0.00	0.02	0.00	0.39	1.23	43.23	2299.68	441.78
Eig 6	0.00	0.45	0.01	0.00	0.00	0.02	0.00	0.39	1.23	43.23	2299.68	441.78
Eig 7	37.41	896.18	120.67	17.33	35.20	186.85	11.70	1212.44	171.44	11.50	3.14	1.90
Eig 8	37.41	896.18	120.67	17.33	35.20	186.85	11.70	1212.44	171.44	11.50	3.14	1.90
Eig 9	4.70	62.00	110.76	541.18	804.14	27.23	635.98	52.50	16.00	2.08	0.26	0.50
Eig 10	4.70	62.00	110.76	541.18	804.14	27.23	635.98	52.50	16.00	2.08	0.26	0.50
Eig 11	77.60	86.67	86.70	87.26	87.57	85.99	88.32	88.20	91.10	95.73	103.62	104.44
Eig 12	575.18	48.31	78.53	128.22	154.65	62.50	182.85	40.01	31.67	45.64	62.10	69.21
Eig 13	575.18	48.31	78.53	128.22	154.65	62.50	182.85	40.01	31.67	45.64	62.10	69.21
Eig 14	188.83	118.59	228.91	308.10	345.20	136.51	384.17	55.83	175.88	441.15	599.83	644.54
Eig 15	188.83	118.59	228.91	308.10	345.20	136.51	384.17	55.83	175.88	441.15	599.83	644.54
Eig 16	250.15	264.93	83.57	217.52	359.39	473.77	523.92	277.47	288.21	168.20	468.92	594.11
Eig 17	250.15	264.93	83.57	217.52	359.39	473.77	523.92	277.47	288.21	168.20	468.92	594.11
Eig 18	70.27	135.37	127.13	42.77	123.13	361.71	225.13	86.14	325.96	308.16	589.90	847.31
Eig 19	70.27	135.37	127.13	42.77	123.13	361.71	225.13	86.14	325.96	308.16	589.90	847.31
Eig 20	7.36	25.62	496.06	86.69	124.93	502.86	431.72	45.98	79.98	83.18	42.02	80.26
Eig 21	7.36	25.62	496.06	86.69	124.93	502.86	431.72	45.98	79.98	83.18	42.02	80.26
Eig 22	3.12	11.71	138.52	27.53	27.98	100.37	114.24	164.65	421.52	371.74	165.71	335.04
Eig 23	3.12	11.71	138.52	27.53	27.98	100.37	114.24	164.65	421.52	371.74	165.71	335.04

Table 6.1 B_m Matrix

Looking at the input for the first eigenvalue (row 1), current injection at busses 2, 3, 4, 5, 7, and 8 can affect changes to the eigenvalue. So without battery placement, losing solar irradiance at busses 2-5 and 7-8 will cause the system to become uncontrollable. Placing batteries at these busses will maintain system controllability, even with the loss of sunlight. Not only do non-zeroes matter, but the magnitude of the values are important, because larger values result in a larger change for the same amount of current injection. In the instance of row 1, the element with the largest magnitude is Bus 4.

The same principals can be applied to the entire table. In order to rank the busses for current injection, the magnitude of each element in a column is summed, and the number of non-zero elements are totaled as well. Using these totals, an index for ranking injection locations can be created. The bus with the least non-zero entries is Bus 1, so it does not receive any scaling. Each other bus is scaled by the number of non-zero values above the minimum (19). For instance, Bus 4 has 21 non-zero values which is 2 more than Bus 1, so its scaling factor increases from 1 to 3. The resulting index is the total magnitude of the B_m columns multiplied by the scaling factor. This is shown in Table 6.2.

Bus	1	2	3	4	5	6	7	8	9	10	11	12
# non-0's	19	23	23	21	21	21	21	23	21	21	21	21
(x)	1	5	5	3	3	3	3	5	3	3	3	3
Total	2,388	5,878	3,050	12,196	4,550	3,954	5,123	6,804	3,233	3,048	8,568	6,134
Index	2,388	29,392	15,249	36,589	13,649	11,863	15,368	34,020	9,700	9,144	25,704	18,402

Table 6.2 B_m Index

The busses with the highest values are bus 4, 8 and 2 respectively.

Based on the analysis in this section, Bus 4, Bus 8, and Bus 2 are the best candidates for battery placement. Those busses have the highest index for the B_m matrix, thus giving the best voltage change per current injected and will help maintain controlability. This set of busses also fall into the category of being lightly damped (<0.05) meaning they will respond agressively to distrubances. If energy storage placement is limited to 2 busses, the analysis indicates that the combination of bus 4 and 8 will yield the most stable results. This placement will workout nicely from a geographical stand point as well since bus 4 and bus 8 are on separate radial feeders. If the entire system is covered by clouds, injecting current at two busses that are close together would cause the voltage at far ends of the system to drop father. So by placing energy storage on both radial feeders, voltage drop issues will be mitigated.

7   System Simulation

In order to verify the results of the analysis from the previous section, system simulations are performed. The state space model of the 12 bus system is implemented in MathWorks' Simulink. The A_p and B_p matrices discussed previously are used again here. The C_p matrix, which couples the states to the output is chosen to be a 23 x 23 identity matrix so that our output shows each state in a column matrix. Figure 7.1 shows the Simulink diagram with outputs for all the states.
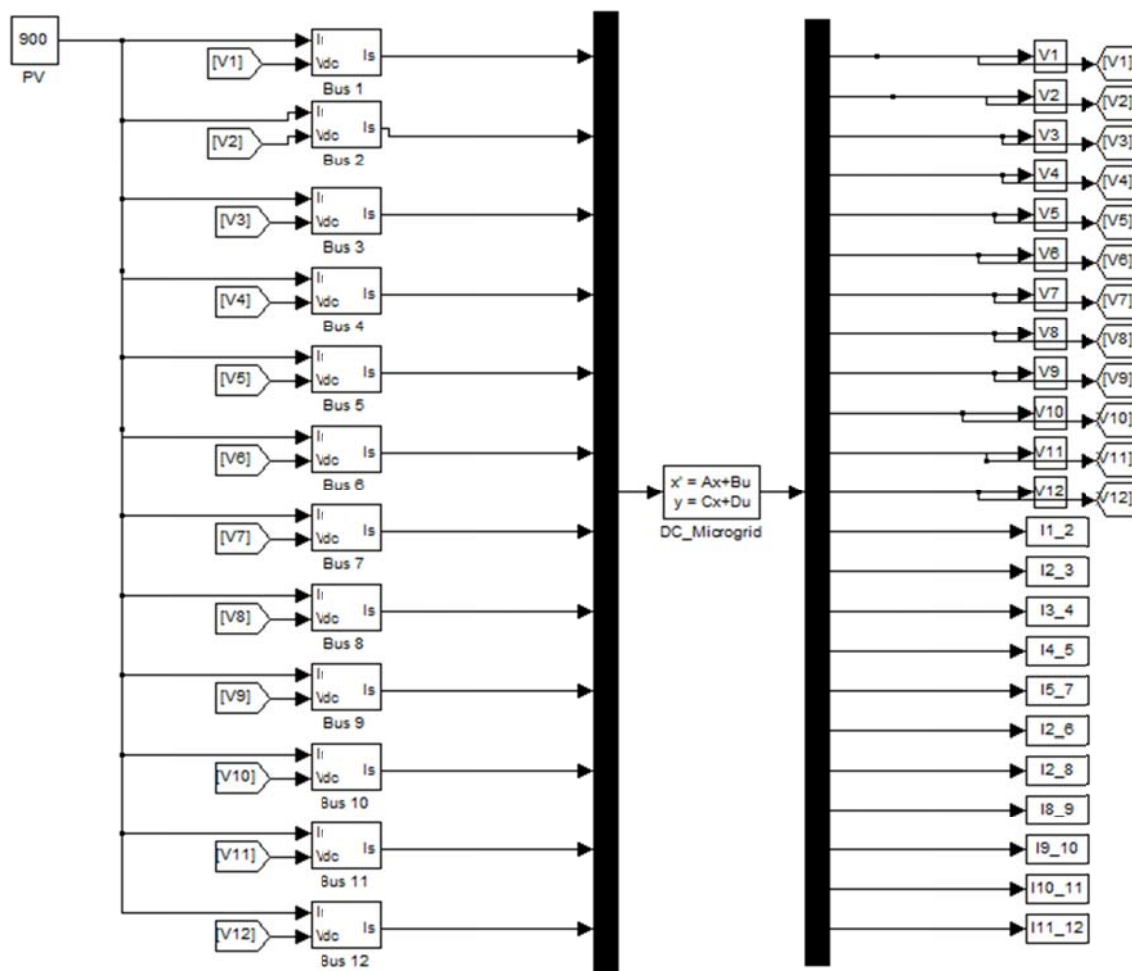

Figure 7.1 Simulink System Model

Each of the input blocks represents current injection at the bus from PV panels and energy storage. The first input to each block is the irradiance in W/m², which is used to estimate the current injection from the solar panels. The second input to the block is node voltage, which the battery controller can use as feedback. Figure 7.2 shows the block diagram for how the inputs are used.
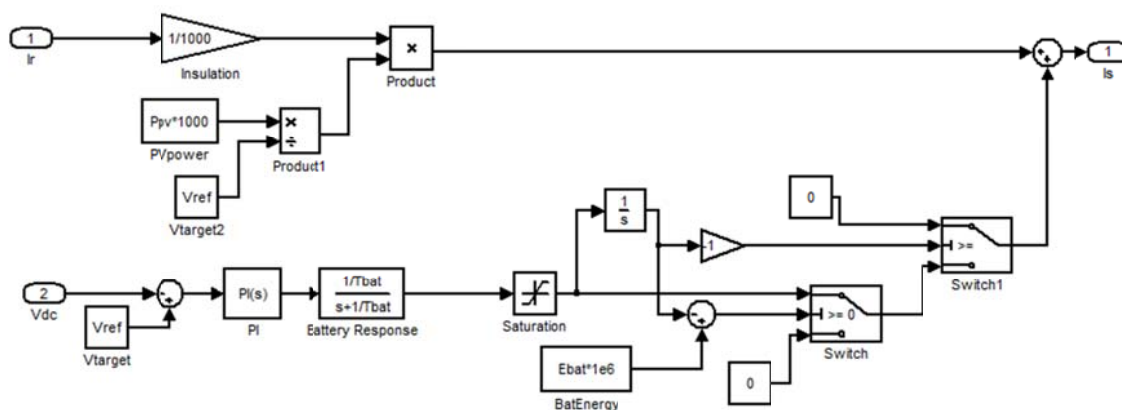

Figure 7.2 Battery and PV Block Model

A PI controller is used with the gains set to Ki = 1000 and Kp = 50. A battery time constant of 1 millisecond is used to account for the fact that the batteries will not respond instantaneously to a change in voltage feedback. Two saturation limits are set so that the batteries output power does not exceed its rating, and so that it does not discharge more energy than is stored.

Now that a model is established, different instability scenarios can be evaluated. The first and most likely is that during the course of the day, cloud cover moves in quickly and prevents the solar panels from supplying power. To simulate this situation, actual PV data will be feed into the input blocks with

different combinations of battery placement. Figure 7.3 shows a sample of actual PV data taken near Milwaukee Wisconsin.
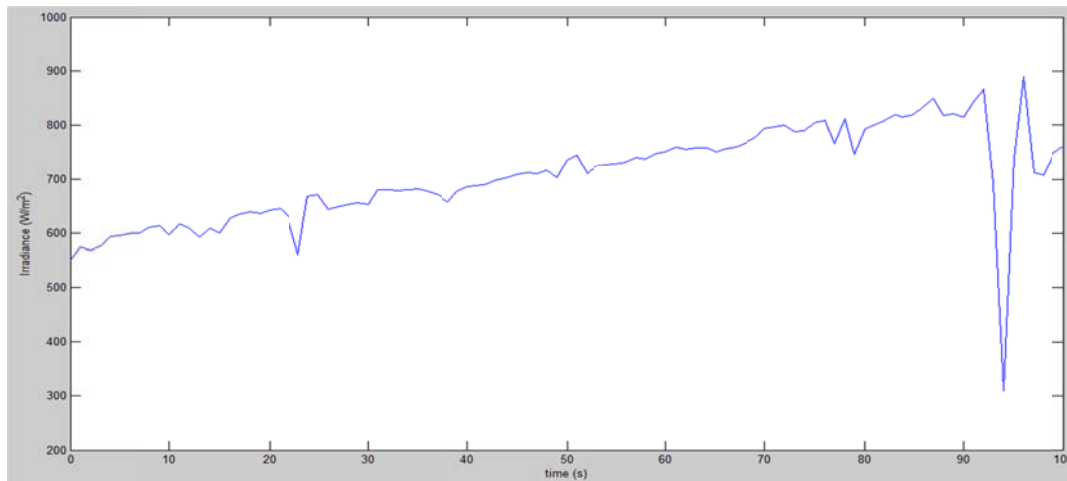

Figure 7.3 PV Irradiance Data

In order to see how the system responds to a dynamic change is PV data, the last 9 seconds, which has a large 600+ irradiance spike, will be used. The simulation is run with different combinations of battery placement. Two groups of 3000 kW batteries are used. The voltage change at each bus is recorded, and shows the average change in voltage at each bus.

	Bus 1	Bus 2	Bus 3	Bus 4	Bus 5	Bus 6	Bus 7	Bus 8	Bus 9	Bus 10	Bus 11	Bus 12
Bus1	26.72	26.81	25.92	25.89	27.82	26.84	25.84	26.83	26.83	26.83	19.02	14.14
Bus 2	26.81	17.58	11.72	11.35	12.69	12.83	13.34	11.50	12.82	12.30	13.44	13.71
Bus 3	26.92	11.72	20.06	14.38	15.99	12.66	17.02	11.58	11.53	12.31	13.83	14.23
Bus 4	25.89	11.35	14.38	23.18	19.45	12.58	20.81	11.36	11.97	12.19	13.92	14.51
Bus 5	27.82	12.69	15.99	19.45	27.54	14.45	24.92	13.04	12.24	13.48	16.54	16.97
Bus 6	26.84	12.83	12.66	12.58	14.45	21.60	14.53	16.30	16.35	13.26	14.91	15.34
Bus 7	25.84	13.34	17.02	20.81	24.92	14.53	33.55	12.80	14.36	14.71	17.97	19.07
Bus 8	26.83	11.50	11.58	11.36	13.04	16.30	12.80	18.86	13.00	13.87	15.07	15.34
Bus 9	26.83	12.82	11.53	11.97	12.24	16.35	14.36	13.00	21.87	17.67	18.73	20.05
Bus 10	26.83	12.30	12.31	12.19	13.48	13.26	14.71	13.87	17.67	29.80	27.97	30.16
Bus 11	19.02	13.44	13.83	13.92	16.54	14.91	17.97	15.07	18.73	27.97	43.54	41.57
Bus 12	14.14	13.71	14.23	14.51	16.97	15.34	19.07	15.34	20.05	30.16	41.57	48.56
Average	25.04	14.18	15.18	15.97	17.93	15.97	19.08	14.96	16.45	18.71	21.38	21.97

Table 7.1 Average Voltage Change for PV Drop

Each element in the table corresponds to 3000 kW of batteries placed at the bus listed in the row header and in the column header. Along the diagonal, where the row and column headers are the same, the value represents voltage change for the placement of two sets of 3000 kW batteries at the same bus. Looking at the results, combinations of busses 2, 4, and 8 provided the lowest average change in voltage. Figure 7.4 shows that without batteries the system's voltage swings can be quite erratic.
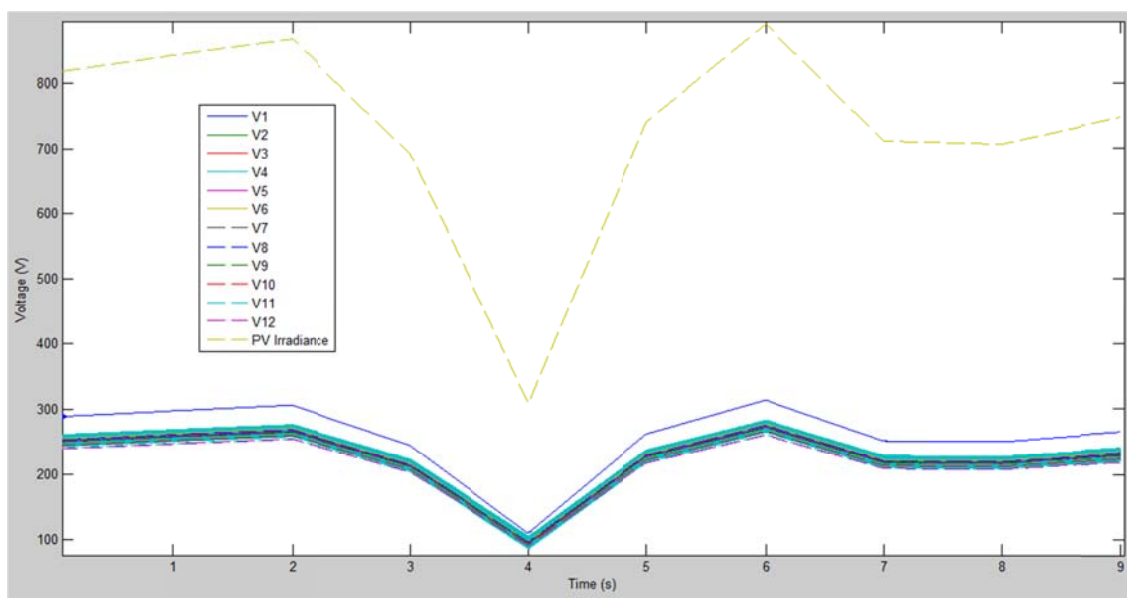

Figure 7.4 Voltage Changes from Irradiance with no Batteries

Figure 7.5 shows the results for a non-ideal placement of batteries at Bus 10 and Bus 11.
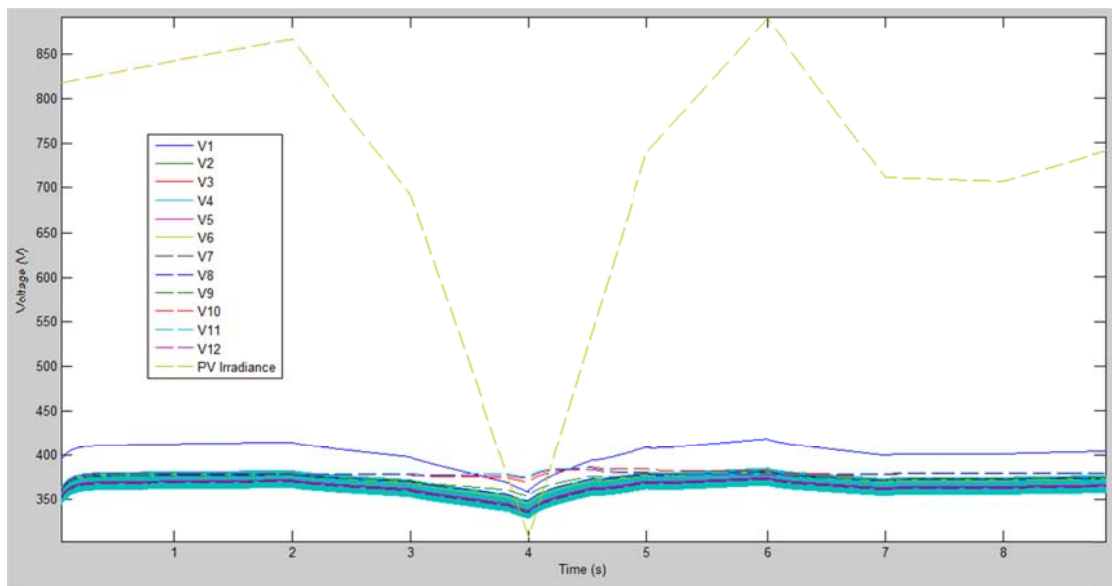
Figure 7.5 Voltage Simulation for PV Drop and Batteries at Bus 10 and 11

Figure 7.6 plots the 12 node voltages and irradiance with batteries placed at bus 4 and 8. This placement maintains the bus voltages throughout the PV irradiance drop.
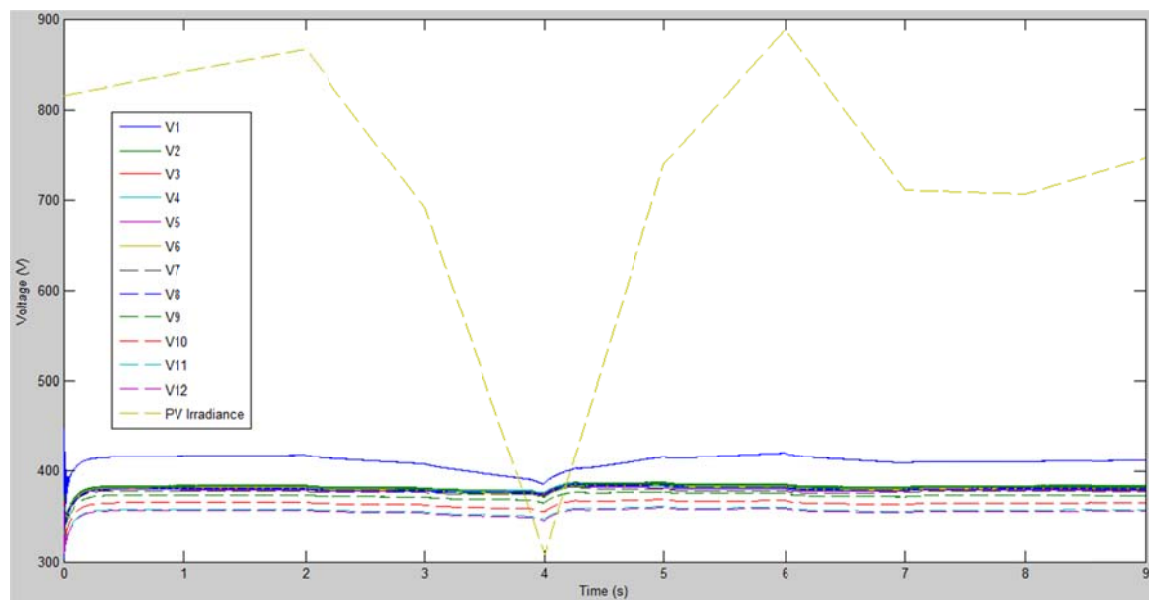

Figure 7.6 Voltage Simulation with PV Drop and Batteries at Busses 4 and 8

Another possible system disturbance is an increase in load. Changing the load affects the system A_p matrix. In order to see the effect of a change in load, the system will have its initial conditions set to the steady state values under normal loading conditions. The system A_p matrix will then be updated, and the simulation will show the results. A 5% increase in load is chosen at each bus. While a single step load at an individual bus is a more likely event, battery placement at that bus will always provide the best support. Since locations of step loads are often always know, a uniform load increase is applied, allowing the busses to be evaluated independently. Table 7.2 tabulates the average voltage change at each bus for varies placements of batteries. As in the previous simulations with changes in irradiance, the element that falls under the column heading and across from a row heading indicates that 3,000 kW of batteries are placed at each bus.

	Bus 1	Bus 2	Bus 3	Bus 4	Bus 5	Bus 6	Bus 7	Bus 8	Bus 9	Bus 10	Bus 11	Bus 12
Bus1	11.66	13.24	13.36	12.46	15.54	13.62	11.30	13.20	13.26	13.42	10.58	10.64
Bus 2	13.24	11.68	9.86	8.82	10.41	9.99	9.79	8.91	10.19	10.15	9.90	9.89
Bus 3	13.36	9.86	12.07	9.21	10.68	9.98	9.41	9.60	9.73	9.80	12.09	9.83
Bus 4	12.46	8.82	9.21	11.18	9.69	9.17	9.84	8.38	8.92	9.04	11.16	8.96
Bus 5	15.54	10.41	10.68	9.69	12.65	9.47	11.35	8.89	8.87	9.62	12.71	10.50
Bus 6	13.62	9.99	9.98	9.17	9.47	11.97	9.22	9.91	10.13	10.23	12.02	10.16
Bus 7	11.30	9.79	9.41	9.84	11.35	9.22	12.87	8.90	9.47	9.85	12.89	10.19
Bus 8	13.20	8.91	9.60	8.38	8.89	9.91	8.90	11.70	10.16	10.52	11.85	10.01
Bus 9	13.26	10.19	9.73	8.92	8.87	10.13	9.47	10.16	12.26	10.94	12.23	10.55
Bus 10	13.42	10.15	9.80	9.04	9.62	10.23	9.85	10.52	10.94	13.12	13.13	11.47
Bus 11	10.58	9.90	12.09	11.16	12.71	12.02	12.89	11.85	12.23	13.13	14.32	14.06
Bus 12	10.64	9.89	9.83	8.96	10.50	10.16	10.19	10.01	10.55	11.47	14.06	14.06
Average	12.69	10.23	10.47	9.74	10.86	10.49	10.42	10.17	10.56	10.94	12.25	10.86

Table 7.2 Average Voltage Change for 5% Load Increase

The various combinations of busses 2, 4, and 8 have the lowest average change in voltage. Figure 7.7 shows the simulation results with no batteries.
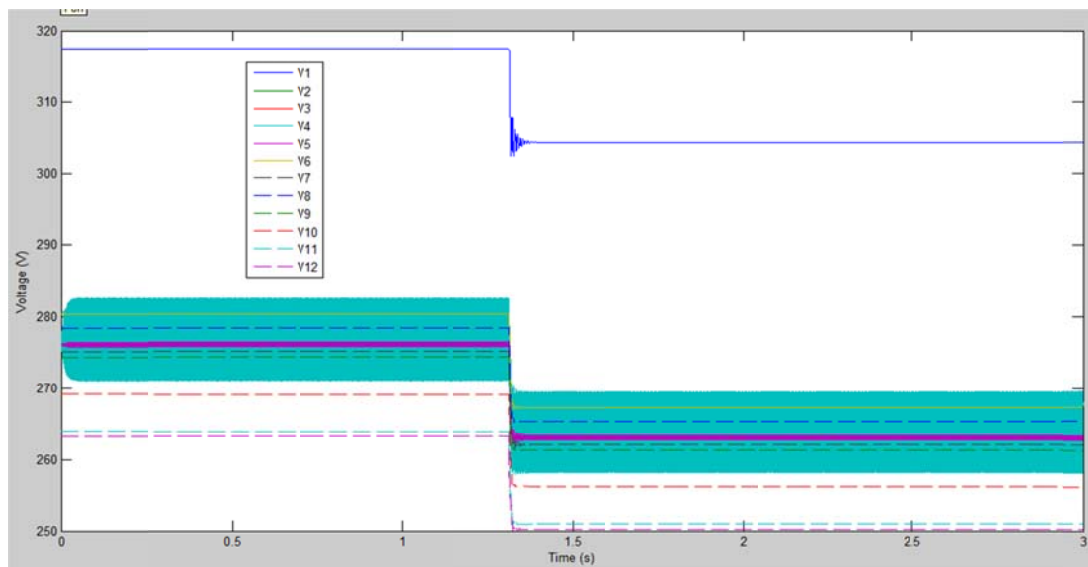

Figure 7.7 Voltage Simulation, Load ↑ and no Batteries

Figure 7.8 plots the voltages for a 5% stepped load increase with batteries at bus 10 and 11. The overall voltage drop is lower with the batteries.
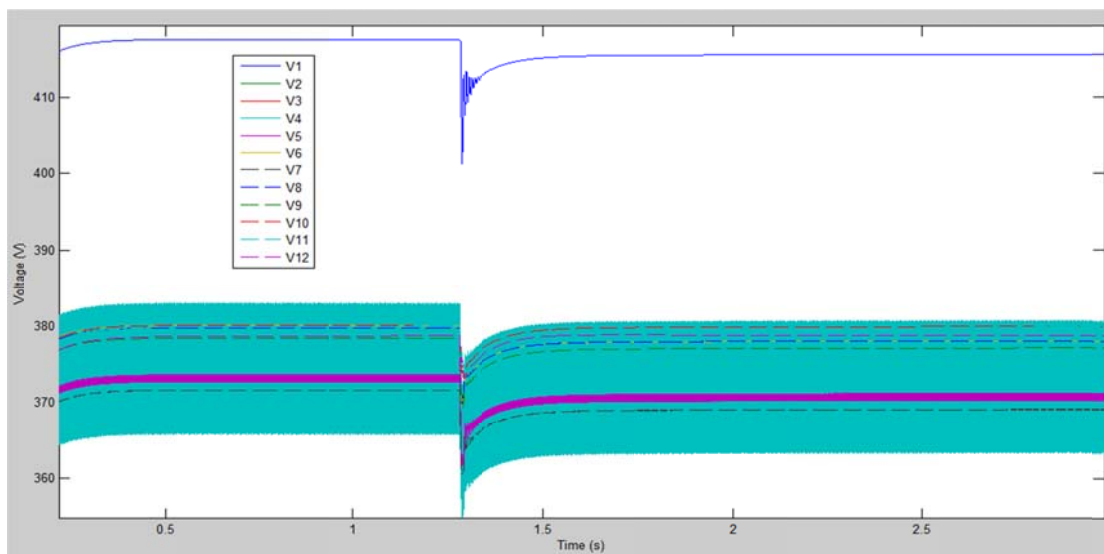

Figure 7.8 Voltage Simulation, Load ↑ and Batteries at Busses 10 and 11

Figure 7.9 shows an example simulation with batteries at bus 4 and bus 8. The results of this simulation clearly provide the lowest voltage swing and also help the system voltages to return to the original value after the step load change.
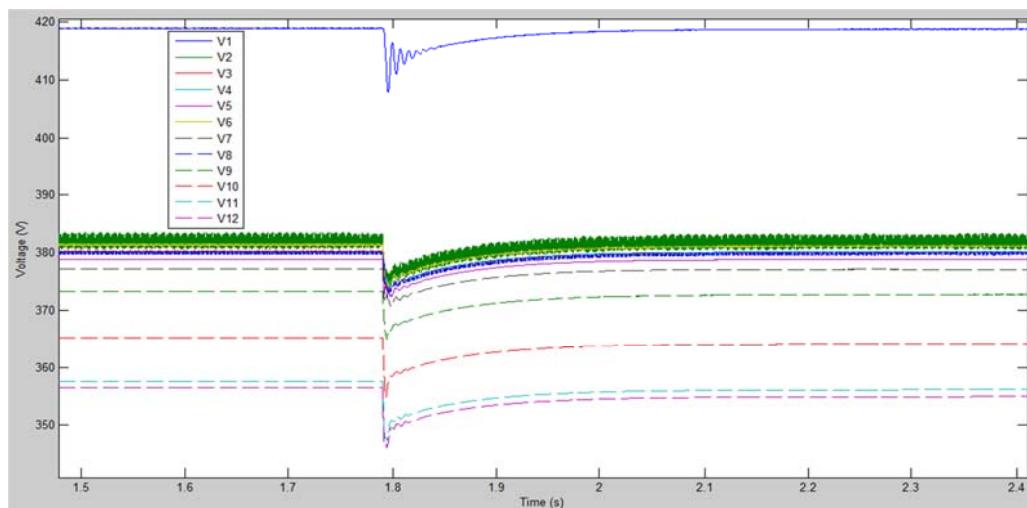

Figure 7.9 Voltage Simulation, Load ↑ and Batteries at Busses 4 and 8

Now that a step increase in load has been simulated, a step decrease in load must also be evaluated. The system is again initialized to normal loading conditions, and the system matrix is updated with the decrease in loading. Table 7.3 shows the average voltage change for different combinations of battery placement. Again in this case, the placement at busses 2, 4, and 8 provide the best results. A simulation is performed without batteries to illustrate the worst-case scenario. The results of the simulation are shown in Figure 7.10.

	Bus 1	Bus 2	Bus 3	Bus 4	Bus 5	Bus 6	Bus 7	Bus 8	Bus 9	Bus 10	Bus 11	Bus 12
Bus1	12.35	13.85	13.91	12.62	14.70	13.95	12.13	13.82	13.88	13.99	11.16	11.15
Bus 2	13.85	12.22	10.20	9.08	9.18	10.53	10.37	10.18	10.43	10.24	9.92	9.99
Bus 3	13.91	10.20	12.70	9.59	10.26	10.47	10.87	9.97	10.06	9.95	9.92	10.07
Bus 4	12.62	9.08	9.59	11.79	10.13	9.56	10.39	8.80	9.11	9.12	9.09	9.19
Bus 5	14.70	9.18	10.26	10.13	13.25	9.65	11.84	9.18	9.86	10.05	10.09	10.20
Bus 6	13.95	10.53	10.47	9.56	9.65	12.59	9.59	10.55	10.59	10.56	10.29	10.35
Bus 7	12.13	10.37	10.87	10.39	11.84	9.59	13.54	9.38	10.00	10.28	10.44	10.54
Bus 8	13.82	10.18	9.97	8.80	9.18	10.55	9.38	12.25	10.46	10.46	10.11	10.21
Bus 9	13.88	10.43	10.06	9.11	9.86	10.59	10.00	10.46	12.86	11.10	10.77	10.88
Bus 10	13.99	10.24	9.95	9.12	10.05	10.56	10.28	10.46	11.10	13.81	11.91	12.04
Bus 11	11.16	9.92	9.92	9.09	10.09	10.29	10.44	10.11	10.77	11.91	14.62	13.33
Bus 12	11.15	9.99	10.07	9.19	10.20	10.35	10.54	10.21	10.88	12.04	13.33	14.83
Average	13.13	10.52	10.66	9.87	10.70	10.72	10.78	10.45	10.83	11.13	10.97	11.07

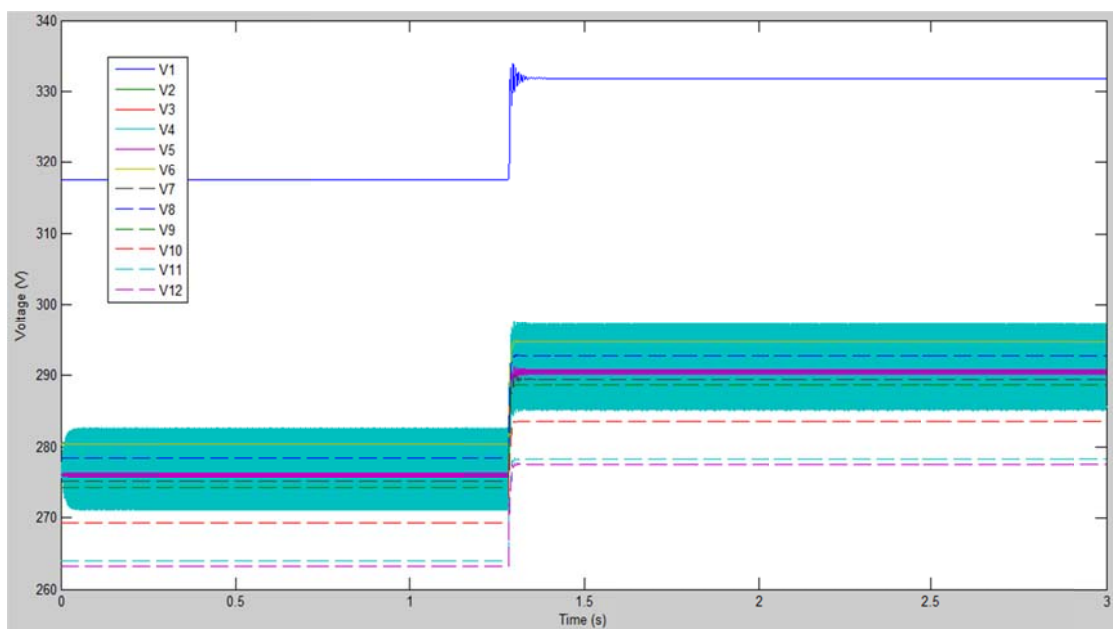**Table 7.3 Average Voltage Change for 5% Load Decrease**

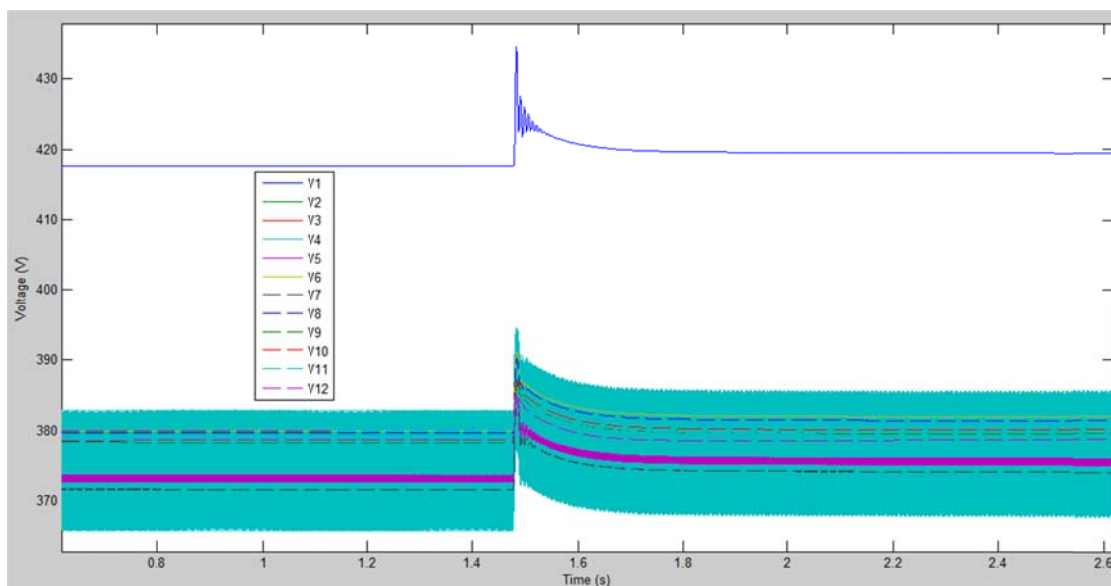**Figure 7.10 Voltage Simulation, Load ↓ and no Batteries**

Figure 7.11 Voltage Simulation, Load ↓ and Batteries at Busses 10 and 11

Figure 7.11 demonstrates the improved system performance of adding batteries, but results are far from ideal. The results of the simulation with the optimal placement of batteries are shown in Figure 7.12.
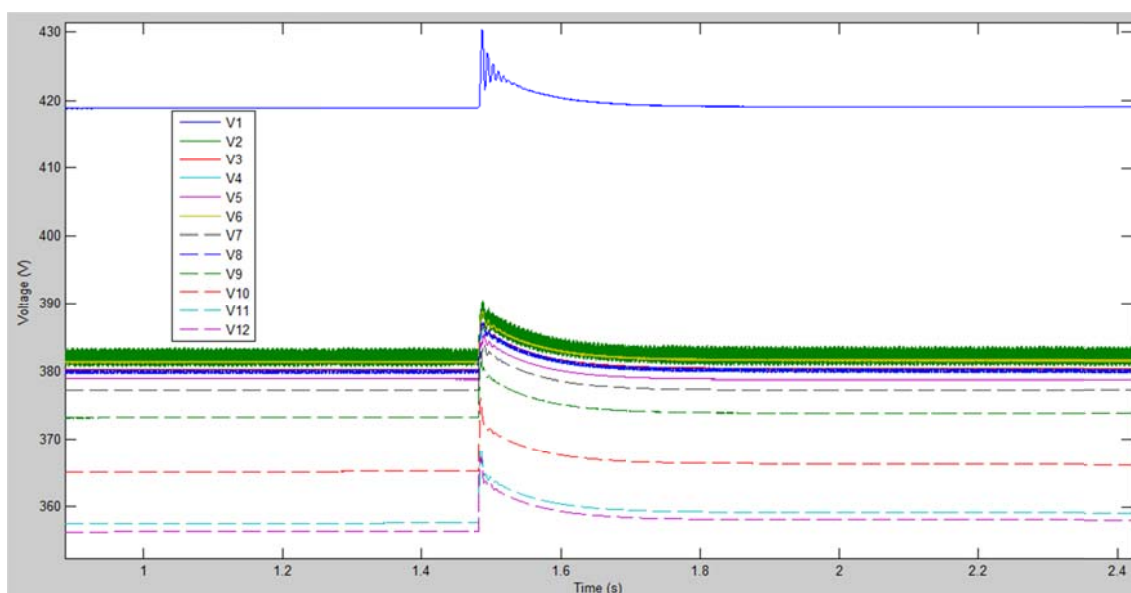

Figure 7.12 Voltage Simulation, Load ↓ and Batteries at Busses 4 and 8

The complete simulation results show that the best location for energy storage placement is at bus 4 and bus 8. Bus 2 is also identified as another promising location. As seen in Table 7.4 they have the lowest average change for both stepped load changes and finish as a close second for changes in irradiance. Of all the simulations run, bus 4 and bus 8 have the lowest average.

	2,4	2,8	4,8	4,9	5,9	3,8	3,9	4,9	4,11
Normal	11.35	11.5	11.36	11.97	12.24	11.58	11.53	11.97	13.92
5% Load ↑	8.82	8.91	8.38	8.92	8.87	9.6	9.73	8.92	12.71
5% Load ↓	9.08	10.18	8.8	9.11	9.86	9.97	10.06	9.11	9.09
Average	9.75	10.20	9.51	10.00	10.32	10.38	10.44	10.00	11.91

Table 7.4 Average Voltage Change for Most Interesting Busses

Other bus locations with low average changes were included as well for reference points.

As predicted by the analysis, bus 2 and 4 finished as another possible candidate, but the placement at bus 4 and 8 is farther apart geographically and helps lower voltage drop across the system. Another possible solution would be to spread the energy storage across all three busses in order to provide better distribution. Figure 7.13 also shows a summary of the various busses of interest.
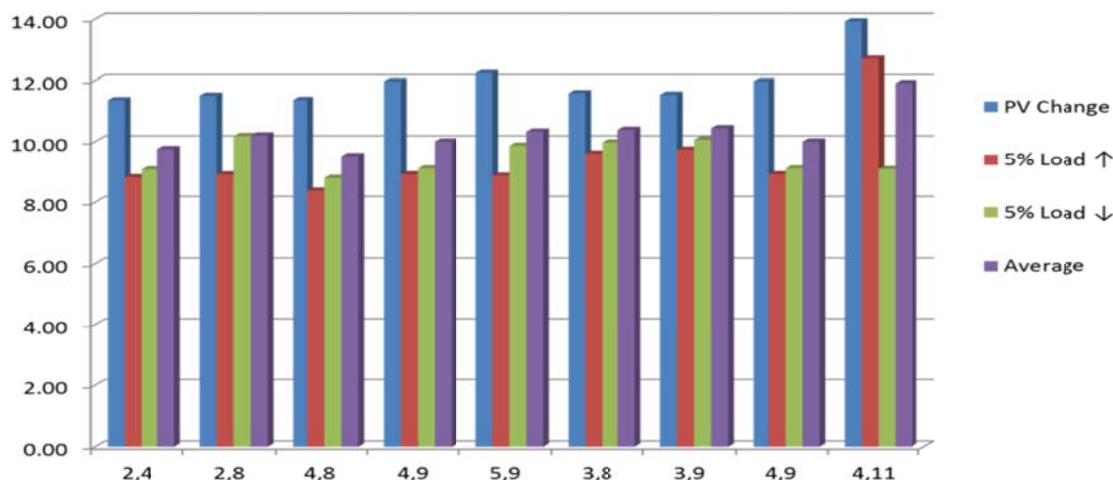
Figure 7.13 Voltage Change Summary

Another important consideration is the effect of stepped load changes on the stability and dynamics of the system. For large enough changes to the loads, the system may behave drastically different. In fact, large changes in load should be treated as a brand new system, and the analysis should be redone. In the instance of ±5% load changes, the system remains relatively the same. Figure 7.14 shows the eigenvalues for both cases. The largest change occurred at the most stable and one of the fastest pairs of eigenvalues (bus 5 and 6). Since this pair is not the dominant mode of the system, the dynamics should remain basically the same and analysis valid.
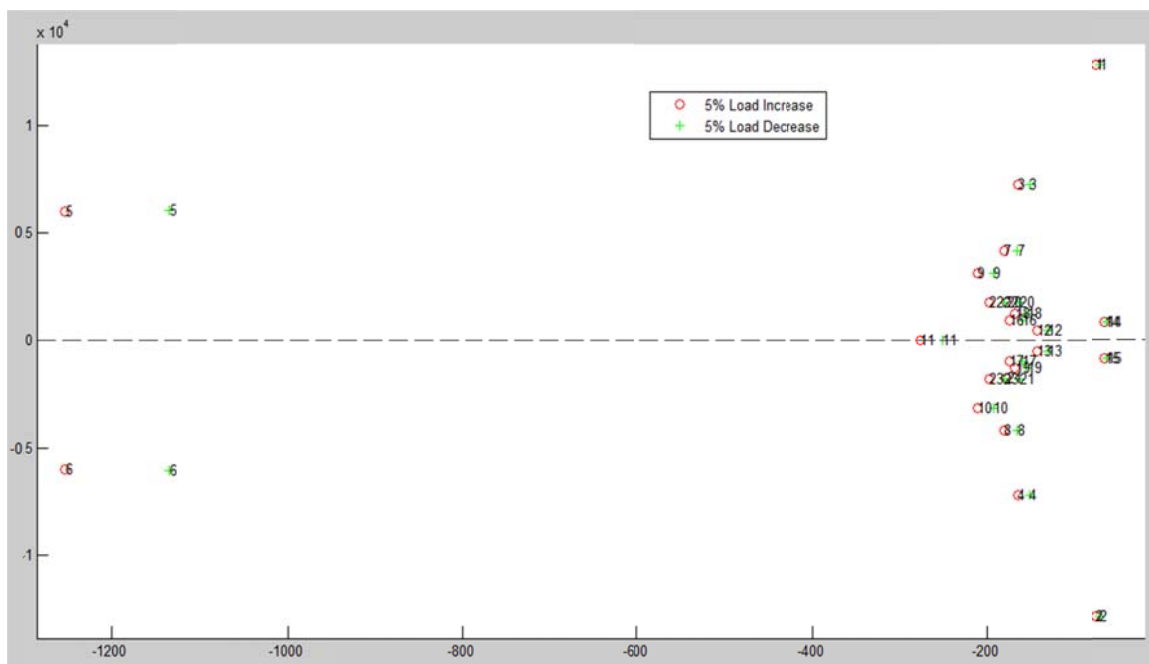
Figure 7.14: System Eigenvalue Changes with Load Variation

In all cases, the eigenvalues moved left, farther away from the left half plane, and

became more stable for the increase in load.

8 Conclusion

The driving factors for the research presented in this thesis are the potential energy efficiency benefits of a DC Microgrid, and the importance of maintaining system stability. The loss of a system can be dangerous and at the very least is costly to the utility that owns it. Frequent outages will frustrate customers. Optimal placement of energy storage will help reduce costs and ensure that the system is operational for longer. In order to prevent outages analysis needs to be performed on system models. Creating system models can be difficult early in a project, but is crucial for proper planning.

This paper uses a very practical approach, grounded in the physical system layout, to model a DC microgrid. Building square footage is used to estimate loads and PV source sizes. System interconnection cables are estimated using distances from overhead maps. The system is designed with large quantities of renewable energy from solar on the roofs of buildings, to off-shore wind turbines in Lake Michigan. In order for such a system to be successful, energy storage measures will need to be added in order to maintain system stability.

The system analysis takes a look at stability using the system model created. The analysis focuses on the eigenvalues for node stability as well as the input matrix for the locations which have the highest impact on bus voltages. The eigenvalue analysis uses the damping and speed of the eigenvalues to determine busses that are most easily changed by disturbances. The input matrix

analysis looks at the input matrix (B_m) converted to modal coordinates with all the modes of the system decoupled. The method of indexing the input matrix sums the magnitude of the columns and weights the sum according to the number of non-zero elements. The goal of analyzing the B_m matrix is to both identify busses where the amount of current injection has the greatest effect on the modes of the system and can affect as many modes as is possible.

In a microgrid with a high penetration of renewable energy, fluctuations in sources are expected in addition to stepped load changes that all electrical systems experience. The analysis is evaluated using simulations of a drop in PV irradiance, 5% stepped load increase, and 5% step load decrease. In each of the simulations 3,000 kW is placed at 2 busses, and the results of every two bus combination are tabulated. Overall, the system simulations confirm the predictions of the system analysis. The tools used in the analysis and modeling sections are ways that designers can create better models, and the methods should help with the planning of future projects.

9 References

[1]   S. Anand, B. Fernandes, "Reduced Order Model and Stability Analysis of Low Voltage DC Microgrid," IEEE Transactions on Industrial Electronics, vol. 99.

[2]   H. Seneff, "Study of the Method of Geometric Mean Distances Used in Inductance Calculation," M.S. thesis, University of Missouri, United States,1947.

[3]   *NFPA 70, The National Electrical Code.* 2008 Edition. Quincy, MA: National Fire Protection Agency, 2007.

[4]   A. Bhatia, "HVAC Refresher - Facilities Standard for the Building Services (Part 2)." Internet: http://www.pdhcenter.com/courses/m216/m216content.pdf, [2012].

[5]   J. Salasovich, G. Mosey, "Feasibility Study of Economics and Performance of Solar Photovoltaics at the Refuse Hideaway Landfill in Middleton, Wisconsin." *NREL*, Internet: http://www.nrel.gov/docs/fy11osti/49846.pdf, [August 2011].

[6]   Q. Hengsi, J. Kimball, "Generalized Average Modeling of Dual Active Bridge DC–DC Converter," *IEEE Transactions on Power Electronics*, vol. 27, no.4, pp. 2078-2084, April 2012.

[7]   H. Krishnamurthy, R. Ayyanar, "Building Block Converter Module for Universal (AC-DC, DC-AC, DC-DC) Fully Modular Power Conversion Architecture," *IEEE Power Electronics Specialists Conference, 2007*, pp. 17-21, June 2007.

[8]   A. Fukyui et. al, "HVDC Power Distribution Systems for Telecom sites and Data Centers" in 2010 International Power Electronics Conference, ISBN 978-1-4244-5393-1/10, p.p. 874-880.

[9]   S. Anand, B. Fernandes, "Optimal Voltage Level for DC Microgrids", ISBN 978-1-4244-5226-2/10, pp. 3034-3039.